J Appl Electrochem (2008) 38:1609–1621
DOI 10.1007/s10800-008-9604-5

ORIGINAL PAPER

Computational and electrochemical investigation for corrosion inhibition of nickel in molar nitric acid by piperidines

K. F. Khaled · Mohammed A. Amin

Received: 5 February 2008 / Accepted: 19 May 2008 / Published online: 5 June 2008

Abstract The adsorption and corrosion inhibition behaviour of four selected piperidine derivatives, namely piperidine (pip), 2-methylpiperidine (2mp), 3-methylpiperidine (3mp), and 4-methylpiperidine (4mp) at nickel in 1.0 M HNO_3 solution were studied computationally by the molecular dynamics simulation and quantum chemical calculations and electrochemically by Tafel and impedance methods. The results indicate a strong dependence of the inhibition performance on the nature of the metal surface, in addition to the structural effects of piperidines. Inhibition is accomplished by adsorption of piperidines on the metal surface without detectable changes in the chemistry of corrosion. Adsorption is predominantly chemisorptive in the active region and by hydrogen bond formation in the passive region. The potential of zero charge (PZC) of the nickel electrode was determined in 1.0 M HNO_3 solutions in the absence and presence of 10^{-2} M 2mp, and the electrostatic (physical) adsorption was discussed. The inhibition efficiency of these compounds increases in the order: 4mp > 3mp > 2mp > pip. Molecular simulation studies were applied to optimize the adsorption structures of piperidine derivatives. The nickel/inhibitor/solvent interfaces were simulated and the charges on the inhibitor molecules as well as their structural parameters were calculated in the presence of solvent effects. Quantum chemical calculations based on the ab initio method were performed to determine the relationship between the molecular structure of piperidines and their inhibition efficiency. Results obtained from Tafel and impedance methods are in good agreement and confirm theoretical studies.

Keywords Molecular dynamic simulation · Quantum chemical calculations · Molecular adsorption · Acid corrosion inhibition · Impedance

K. F. Khaled (✉)
Electrochemistry Research Laboratory, Chemistry Department, Faculty of Education, Ain Shams University, Roxy, Cairo, Egypt
e-mail: khaled@asunet.shams.edu.eg

M. A. Amin
Chemistry Department, Faculty of Science, Ain Shams University, Abbassia, Cairo, Egypt

1 Introduction

The adsorption of inhibitor molecules on surfaces has recently become the subject of intensive investigation in the corrosion field because of the wealth of information that can be obtained [1–3]. Understanding how an inhibitor molecule behaves near a metal surface will greatly enhance the ability to control the essential interfacial properties in a wide variety of corrosion problems. Several computational and electrochemical methods have been used to study the behaviour of inhibitors for different metals [4–6].

The corrosion behaviour of nickel in acid baths in plating, electrowining and pickling process is of industrial concern. Although the mechanism of corrosion and inhibition of nickel has been studied in different media [7–10], studies in nitric acid in the presence of organic molecules are rare [10]. Kumar et al. [12] studied the corrosion inhibition of nickel using different thiones in 4% nitric acid at different temperatures. The inhibition efficiencies of thiones are determined by the electrochemical technique (potential decay experiments) and carried out to determine the relative stability of the passive film formed on the nickel surface in the presence and absence of thiones. The electrochemical investigations of nickel in a wide range of concentrations (1–14.6 M) of nitric acid were studied by

various electrochemical techniques as well as the chemical (weight loss) method. [13]. The inhibiting action of alkyl triphenyl phosphonium iodine salt towards the corrosion behaviour of nickel in 1 M H_2SO_4 solution has been studied [14] This compound was found to retard both the anodic and cathodic reactions of nickel corrosion.

The aim of this work is to study the influence of four selected piperidines, namely piperidine (pip), 2-methylpiperidine (2mp), 3-methylpiperidine (3mp), 4-methylpi peridine (4mp), on the inhibition of nickel corrosion in 1.0 M HNO_3 solutions using electrochemical techniques (polarization and impedance) as well as explicit solvent simulations using molecular dynamics and quantum chemical calculation to explore the adsorption mechanism of piperidines on nickel (1 0 0). Also, as the electronic structure of piperidines could be involved in determining interactions with the nickel surface, correlation between molecular orbital calculations and inhibitor efficiencies will be sought. Adsorption via hydrogen bonding is also discussed.

2 Experimental

The nickel electrode used was of 99.999 % purity (Johnson Matthey Chemicals). The nickel rod was welded to an iron-wire for electrical connection and mounted in Teflon with an active flat disc shaped surface of (1.0 cm^2) geometric area to contact the test solution. Prior to each experiment the nickel electrode was polished with different grit sizes emery papers up to 4/0 grit size to remove the corrosion products, if any, formed on the surface. The nickel electrode was cleaned in 18 MΩ water in an ultrasonic bath for 5 min. and subsequently rinsed in acetone and bi-distilled water and immediately immersed in the test solution.

The heterocyclic amines studied are presented below:

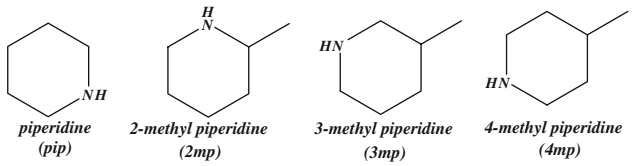

piperidine (pip) *2-methyl piperidine (2mp)* *3-methyl piperidine (3mp)* *4-methyl piperidine (4mp)*

All of these compounds were obtained from Aldrich Chemical Co. They were added to the 1.0 M HNO_3 (Fisher Scientific) without pre-treatment at concentrations of 10^{-4}, 10^{-3}, 5×10^{-3}, and 10^{-2} M. The electrode was immersed in these solutions for 1 h before starting measurements; this was the time necessary to reach a quasi-stationary value for the open circuit potential.

A conventional electrochemical cell of capacity 250 ml was used containing three compartments for working, platinum mesh counter and reference electrodes. A Luggin-capillary was also included in the design, the tip of which was positioned very close to the surface of the nickel electrode to minimize IR drop. The reference electrode was a saturated calomel electrode (SCE) used directly in contact with the test solution. The measurements were carried out in aerated non-stirred 1.0 M HNO_3 solutions at 25 °C (using water thermostat ±1 °C) without and with various concentrations (10^{-4} to 10^{-2} M) of piperidine derivatives as possible corrosion inhibitors. All solutions were freshly prepared from analytical grade chemical reagents using doubly distilled water and were used without further purification. For each run, freshly prepared solutions as well as a cleaned set of electrodes were used.

Tafel polarization curves were obtained by changing the electrode potential automatically from (−250 to +250 mV_{SCE}) versus open circuit potential with a scan rate of 1.0 mV s^{-1}. Impedance measurements were carried out in the frequency range 100 kHz to 50 mHz with an amplitude of 5 mV peak-to-peak using ac signals at the corrosion potential (E_{corr}). An impedance experiment was carried out in (1.0 M HNO_3 + 5×10^{-3} M 2mp) solution at an anodic potential of (E_{corr} + 0.20 V), within the potential range of the passive region, to confirm adsorption via hydrogen bonding. Measurements were performed with a Gamry Instrument Potentiostat/Galvanostat/ZRA. This includes a Gamry Framework system based on the ESA400, Gamry applications that include DC105 for dc corrosion measurements, EIS300 for impedance measurements to calculate the corrosion current and the Tafel constants along with a computer for collecting the data. Echem Analyst 4.0 Software was used for plotting, graphing and fitting data.

The molecular dynamics (MD) simulations were performed using the commercial software MS Modeling from Accelrys using the amorphous cell module to create solvent-piperidines cells on the nickel-substrate. The behaviour of the four selected inhibitors (Fig. 1) on the surface was studied using molecular dynamics simulations and the COMPASS force field. COMPASS stands for condensed-phase optimized molecular potentials for atomistic simulation studies. COMPASS is an ab initio powerful force field which supports atomistic simulations of condensed phase materials [15]. Most parameters were derived based on ab initio data. The MD calculation of the simulation of the interaction between the piperidine derivatives dissolved in H_2O and the nickel surface (1 0 0) was carried out in a simulation box ($30 \times 30 \times 29.9$ Å) with periodic boundary conditions in order to simulate a representative part of an interface devoid of any arbitrary boundary effects. A cutoff distance of 1.0 nm with a spline switching function was applied for the non-bond interactions, i.e., for Coulombic, van der Waals and hydrogen bond interactions. The cutoff distance specifies the distance at which to exclude interactions from the non-bond list. The spline switching function is

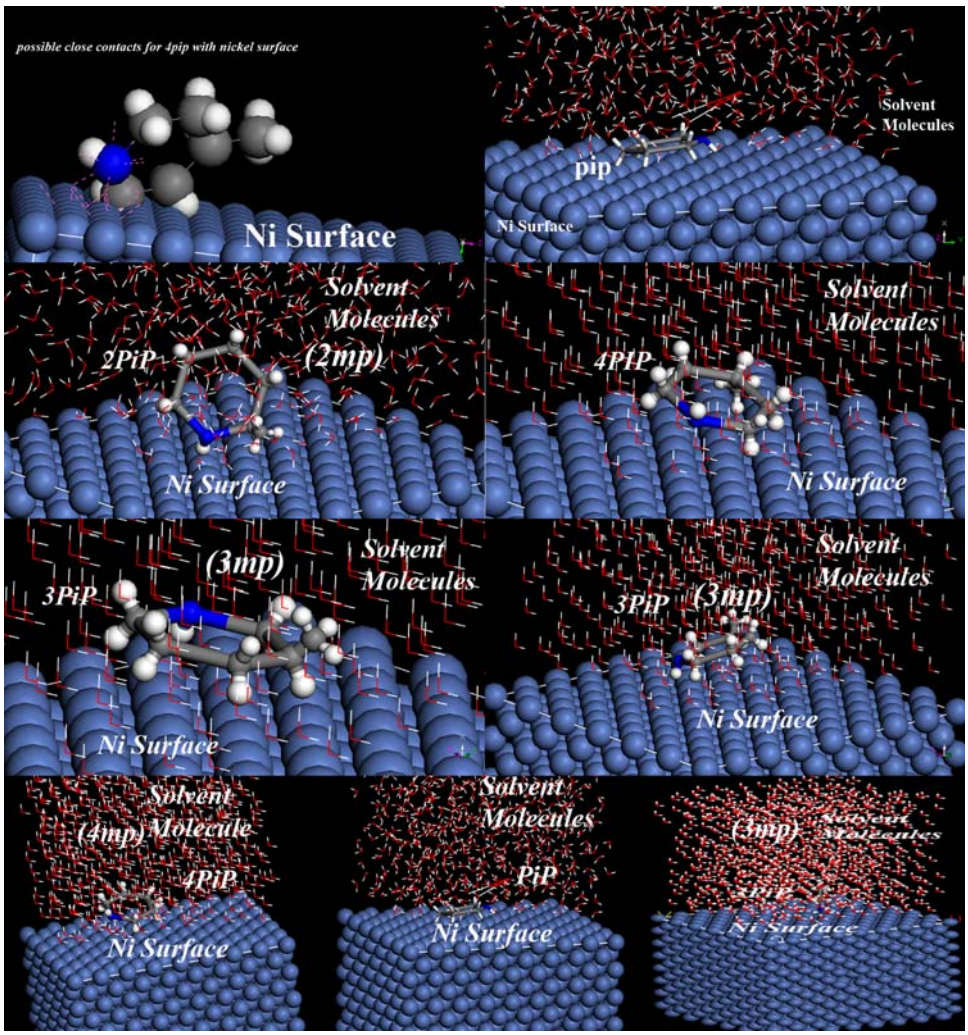

Fig. 1 Representative structures of 3D amorphous cells containing the nickel substrate, the solvent molecules and the piperidine derivatives

used to select the spline width which specifies the size of the region within which non-bond interactions are splined from their full value to zero. For the actual computation of this interaction energy charge groups are used.

The nickel crystal is cleaved along with the (1 0 0) plane, thus representing the nickel surface. For the MD simulation, all the spatial positions of the nickel atoms in the simulation box are fixed because the thermal vibrations of the interaction with an adsorbed molecule and not in the physical behaviour of the crystal itself. The liquid phase consists of 600 H_2O molecules and a single dissolved inhibitor molecule. On the top of this "aqueous layer", an additional layer of 300 H_2O molecules with fixed spatial positions serves as an upper limit for the liquid phase acting like a wall but with the same physical and chemical properties. Before each MD run the inhibitor molecule was located close to the nickel surface because the time scale of such a diffusion process would exceed the time scale of the whole simulation.

For quantum chemical calculations, the study was carried out using Dewar's Linear Combinations of Atomic Orbitals–Self-Consistent Field–Molecular Orbital (LCAO–SCF–MO) [16, 17] ab initio with basis set STO-3G method with commercially available quantum chemical software HyperChem, Release 8.0 [18]. A full optimization of all geometrical variables without any symmetry constraint was performed at the Restricted Hartree–Fock (RHF) level [19, 20]. This develops the molecular orbitals on a valence basis set and also, calculates electronic properties, optimized geometries and total energy of the molecules. As an optimization procedure, the built-in Polak–Ribiere algorithm was used [21].

3 Results and discussions

3.1 Adsorption energy calculations

In the simulation, the piperidines interact with the nickel surface in water at 25 °C. Meanwhile, molecular dynamics simulations are implemented with piperidines in different possible configurations on the nickel surfaces and the

Table 1 Calculated structural parameters using ab initio method

Inhibitor	Piperidine (pip)	2-methyl piperidine (2mp)	3-methyl piperidine (3mp)	4-methyl piperidine (4mp)
Adsorption energy/kJ mol^{-1}	−27.41	−28.01	−28.2	−34.25
E_{HOMO}/eV	−8.881	−8.731	−8.521	−8.169
E_{LUMO}/eV	15.921	15.819	15.531	15.31
ΔE (E_{LUMO}–E_{HOMO})/eV	24.8	24.55	24.05	23.47
$-E_{tot}$/kJ mol^{-1}	649489	750848	750852	759217.5
Calculated hydrogen bond length/Å	2.3	2.01	1.8	1.4
ΔN	0.320	0.323	0.328	0.339

adsorption energy is calculated. So the configuration with the maximal adsorption energy is chosen as the initial simulation states. The piperidines adsorbed on the nickel surfaces after equilibrium is shown in Fig. 1. The maxiumum contact area, which increase the adhesion energy and stabilizes the piperidines on the nickel substrate, are reached with 4-methyl piperidine (4mp).

The adsorption energy of the selected piperidines on nickel and the possible hydrogen bonding formation between the piperidine derivative and the nickel surface are investigated. The adsorption energy of single piperidine derivative on nickel surfaces as well as the calculated hydrogen bond length, Table 1, confirmed that 4-methyl piperidine is adsorbed on the nickel surface more strongly than the other piperidines. These results indicate that the interaction between the four tested inhibitors and the nickel surface is strong and may occur via hydrogen bonding. It follows from the data of Table 1 that 4-methyl piperidine (4mp) possesses the highest adsorption energy on Ni (1 0 0) surface and the shortest hydrogen bond length, suggesting that 4mp is the best inhibitor among the investigated piperidines. Experimental results confirmed adsorption via hydrogen bonding in the passive region (see details in Sect. 3.4.2).

3.2 Quantum chemical calculations

The selection of effective inhibitors for aqueous corrosion of metals has been widely carried out, based on an empirical approach. Some studies on inhibitors from a quantum chemical point of view have been reported [22–25].

In order to investigate the charge distribution of piperidines molecules, ab initio quantum chemical calculations were performed using the Hyperchem 8.0 package. The Mulliken charge distributions of the piperidines molecules as well as the highest occupied molecular orbitals (HOMO) and lowest unoccupied molecular orbitals (LUMO), were calculated, Fig. 2.

It is confirmed that the more negative the atomic partial charges of the adsorbed centre are, the more easily the atom donates its electrons to the unoccupied orbital of the surface atoms of the nickel surface. In Fig. 2 (the numerical values were listed), the atomic partial charges of the nitrogen atom in (methyl piperidines) is −0.326, while that of piperidine itself is −0.321.

It can be seen from Fig. 2 that the electron density distribution is the highest in the case of 4-methyl piperidine, confirming that it is the best inhibitor of the selected piperidines. Some of the key quantum chemical parameters were computed using the ab initio method and these are listed in Table 1. These are mainly the energies of the highest occupied (E_{HOMO}) and lowest unoccupied (E_{LUMO}) molecular orbitals and total energy (E_{tot}). These quantum chemical parameters were obtained after geometric optimization with respect to all nuclear coordinates.

Frontier orbital theory is useful in predicting adsorption centers of the inhibitor molecules responsible for the interaction with surface metal atoms [26, 27]. Terms involving the frontier MO could provide dominative contribution, because of the inverse dependence of stabilization energy on orbital energy difference [26]. Moreover, the gap between the HOMO and LUMO energy levels of the molecules is another important factor that should be considered. Reportedly, excellent corrosion inhibitors are usually those organic compounds which not only offer electrons to unoccupied orbital of the metal, but also accept free electrons from the metal [26, 28].

The quantum chemical calculation in this study revealed that the linear correlation between MO energy level and the corrosion inhibition efficiency proved that the higher the HOMO energy of the inhibitor, the greater the trend of offering electrons to the unoccupied d orbital of the metal, and the higher the corrosion inhibition efficiency for nickel in nitric acid solutions. In addition, the lower the LUMO energy and the smaller the energy gap (E_{LUMO}–E_{HOMO}), the easier the acceptance of electrons from the metal surface, corresponding to increased inhibition efficiency. The number of electrons transferred (ΔN) was also calculated depending on the quantum chemical method, as in Eq. 1:

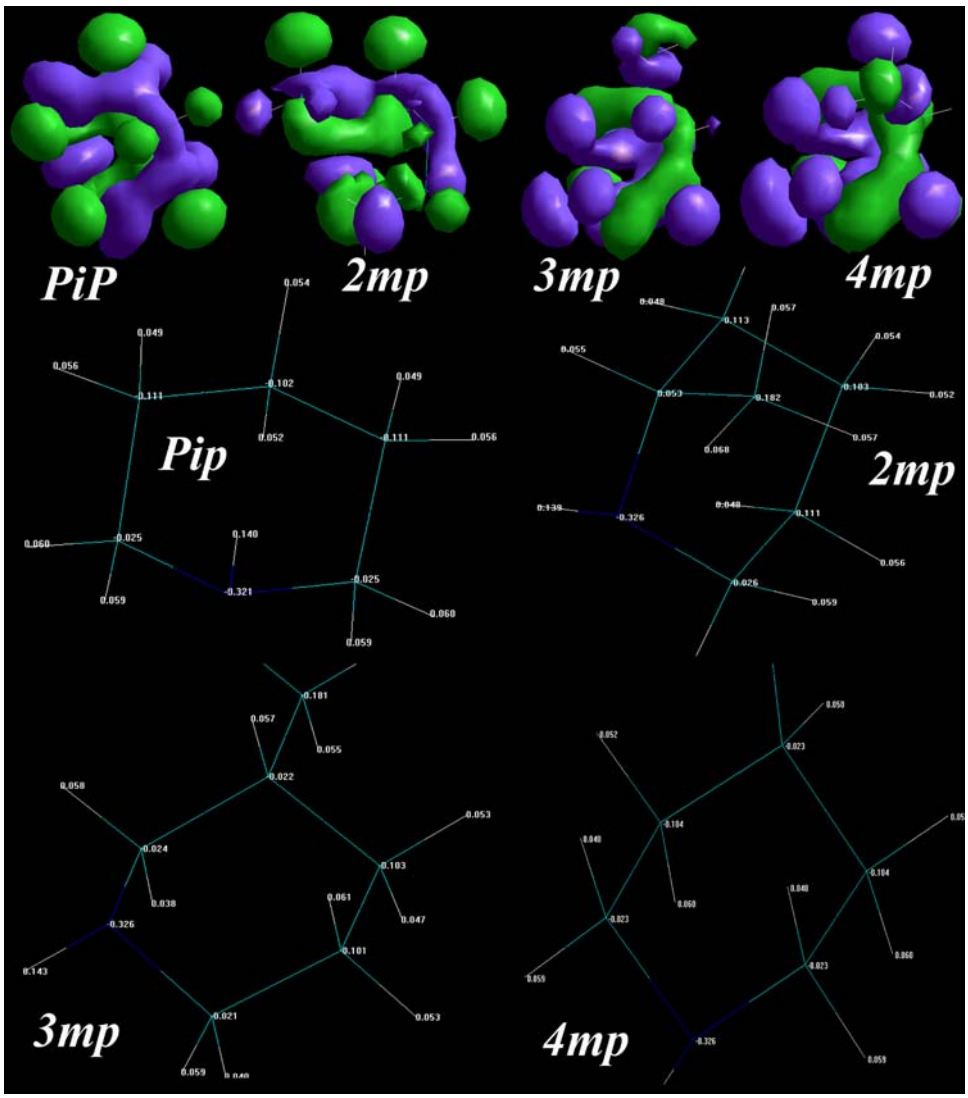

Fig. 2 Structure of triazole derivatives, molecular orbital plots and charge density distribution

$$\Delta N = \frac{\chi_{Ni} - \chi_{inh}}{2(\eta_{Ni} + \eta_{inh})} \quad (1)$$

where χ_{Ni} and χ_{inh} denote the absolute electronegativity of nickel and the inhibitor molecule, respectively; η_{Ni} and η_{inh} denote the absolute hardness of nickel and the inhibitor molecule, respectively. These quantities are related to electron affinity (A) and ionization potential (I) which are useful in their ability to help predicting chemical behaviour [29].

$$\chi = (I + A)/2 \quad (2)$$

$$\eta = (I - A)/2 \quad (3)$$

I and A are related in turn to E_{HOMO} and E_{LUMO}

$$I = -E_{\mathrm{HOMO}} \quad (4)$$

$$A = -E_{\mathrm{LUMO}} \quad (5)$$

Values of χ and η were calculated by using the values of I and A obtained from quantum chemical calculation. Using a theoretical χ value of 4.4 eV/mol according to Pearson's electronegativity scale and η value of 0 eV/mol for nickel [30], ΔN, the number of electrons transferred from inhibitor to the nickel surface, was calculated. Values of ΔN showed that the inhibition effect resulted from electron donation. Agreeing with Lukovits's study [31], if $\Delta N < 3.6$, the inhibition efficiency increased with increasing electron-donating ability at the metal surface. Based on these calculations, it is expected that the four tested piperidines were donors of electrons, and the nickel surface was the acceptor, and this favours chemical adsorption of the inhibitor on the electrode surface. The compounds bind to the nickel surface and form an adsorption layer against corrosion. 4-methy piperidine (4mp) had the highest inhibition efficiency because it had the highest HOMO energy and ΔN values, and it had the greatest ability (the lowest E_{tot}) of offering electrons, and piperidine had the lowest inhibition efficiency, for vice

versa. In Fig. 1, the different views of the adsorption structures of piperidines are shown. It can be seen that the piperidine molecule has a nearly flat orientation with respect to the nickel surface. For (4mp), most of the molecules have a nearly flat orientation with respect to the nickel surface while others (pip, 2mp and 3mp) bond with the nickel surface by tilting at an angle.

3.3 Electrochemical techniques

3.3.1 Tafel extrapolation method

The polarization behaviour of nickel in 1 M HNO_3 solutions in the absence and presence of different concentrations of piperidines at a scan rate of 1 mV s^{-1} and at 25 °C, is shown in Figs. 3–6. The anodic curve corresponds to the electrochemical generation of nickel oxides and/or nitrates. A surface steady state appears indicating that the corrosion products formed at the electrode surface allowed pseudo-passivation of the material [14]. This may account for the appearance of the passivation plateau in the anodic domain. The cathodic domain is due to hydrogen evolution under kinetic-control [14]. The values of the corrosion current density (i_{corr}) for nickel corrosion reaction without and with inhibitors were determined by extrapolation of the cathodic and anodic Tafel lines to the corrosion potential (E_{corr}). Table 2 represents the influence of piperidine concentration on the corrosion parameters. As it can be seen from Figs. 3–6, the anodic and cathodic reactions are affected. Piperidines are thus mixed-type inhibitors, meaning that the addition of these compounds to nitric acid solutions reduces the anodic dissolution of nickel, corresponding to a noticeable decrease in the current densities of the passivation plateau, and also retards the cathodic hydrogen evolution reaction.

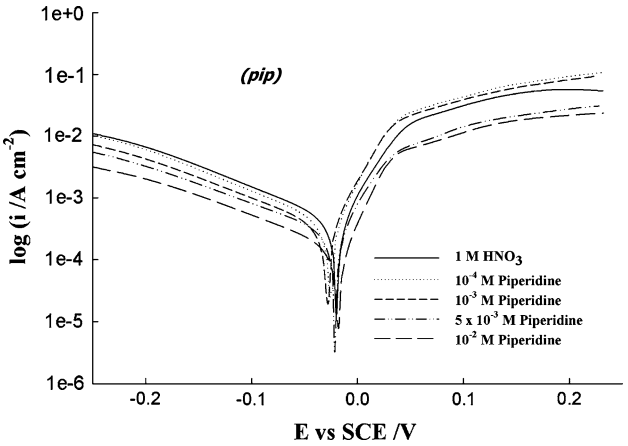

Fig. 3 Tafel polarization curves recorded for nickel electrode in 1.0 M HNO_3 solution without and with various concentrations of piperidine at a scan rate of 1.0 mV s^{-1} and at 25 °C

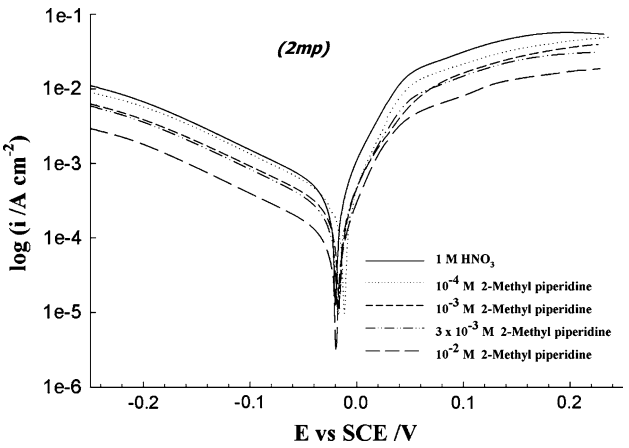

Fig. 4 Tafel polarization curves recorded for nickel electrode in 1.0 M HNO_3 solution without and with various concentrations of 2-methyl piperidine at a scan rate of 1.0 mV s^{-1} and at 25 °C

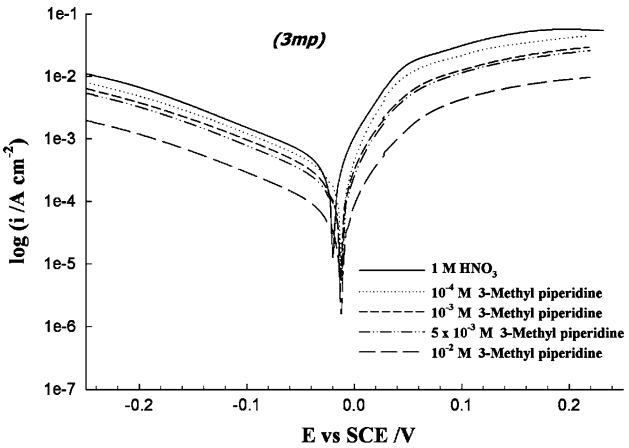

Fig. 5 Tafel polarization curves recorded for nickel electrode in 1.0 M HNO_3 solution without and with various concentrations of 3-methyl piperidine at a scan rate of 1.0 mV s^{-1} and at 25 °C

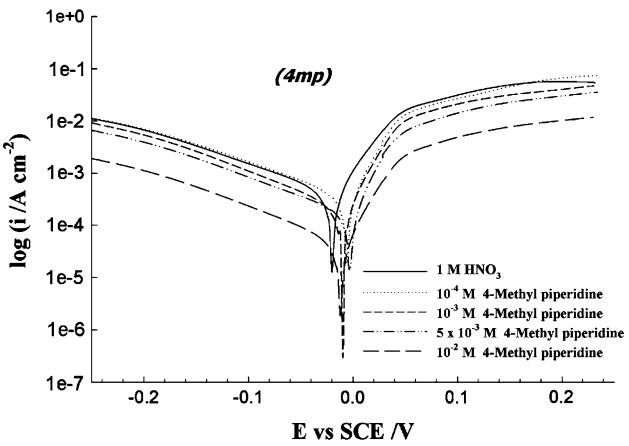

Fig. 6 Tafel polarization curves recorded for nickel electrode in 1.0 M HNO_3 solution without and with various concentrations of 4-methyl piperidine at a scan rate of 1.0 mV s^{-1} and at 25 °C

Table 2 Electrochemical kinetic parameters obtained from Tafel polarization curves shown in Figs. 3–6 for nickel electrode in 1.0 M HNO_3 solution without and with different concentrations of the four tested inhibitors

Inhibitor	Conc./M	i_{corr}/μA cm^{-2}	$-E_{corr}$/mV	b_c/mV dec^{-1}	b_a/mV dec^{-1}	C.R mpy	IE_p%
	Blank	527	19.8	169.1	44.8	223.7	
pip	10^{-4}	430	25.3	167.4	39.6	182.4	18.4
	10^{-3}	384	28.5	169.5	39.9	162.9	27.13
	5×10^{-3}	312	21.5	180.8	41.9	132.6	40.79
	10^{-2}	185	18.3	180.0	39.6	78.38	64.89
2mp	10^{-4}	387	12	166.4	41.1	164.5	26.56
	10^{-3}	325	16.5	167.1	42.1	137.9	38.33
	5×10^{-3}	273	17.7	169.5	41.4	115.9	48.19
	10^{-2}	133	19.2	167	40.4	56.3	74.76
3mp	10^{-4}	351	11.8	171	39.3	149.2	33.39
	10^{-3}	285	13.1	171.4	41	121.2	45.92
	5×10^{-3}	221	12.4	169.9	43.4	93.83	58.06
	10^{-2}	85.9	12.6	170.5	42.7	36.47	83.70
4mp	10^{-4}	313	5.6	167.5	39.9	132.9	40.61
	10^{-3}	261	9.6	169.9	38.9	110.7	50.47
	5×10^{-3}	196	2.84	166	37.5	83.3	62.81
	10^{-2}	59.1	11.7	167.4	39.8	25.08	88.78

The corrosion potentials (E_{corr}) have no definite shift and i_{corr} decreases when the concentration of piperidines is increased. The absence of significant change in the Tafel slopes in the presence of inhibitor indicates that the corrosion mechanism is not changed after adding the inhibitor and the inhibitive effect is attributed to simple adsorption. These results indicate that the electrochemical process at the Nickel–HNO_3 interface is controlled by activation kinetics [14]. The inhibition efficiency, IE(%), was evaluated from the measured i_{corr} values using the relationship:

$$IE_p = \left(1 - \frac{i^{o}_{corr}}{i_{corr}}\right) \times 100 \quad (6)$$

where i^{o}_{corr} and i_{corr} are the corrosion current densities for uninhibited and inhibited solutions, respectively. Data in Table 2 indicate that for all cases the inhibition efficiency values, IE_p%, increased with increase in piperidine concentration. Maximum inhibition efficiency was obtained for 4-methyl piperidine (4mp) at a concentration of 10^{-2} M.

3.3.2 Impedance measurements

In order to gain more information about the corrosion inhibition phenomenon on nickel electrodes by piperidines, impedance measurements were carried out in aerated 1.0 M HNO_3 solution in the absence and presence of the different concentrations of piperidine derivatives at the respective corrosion potentials and at 25 °C. Figure 7 shows the Bode and Bode phase plots recorded without and with various concentrations of piperidines after immersion for 60 min in molar nitric acid solutions. The Bode plots show that the maximum phase angle shifts to lower frequencies and the polarization resistance increases with increasing concentration. In the presence of piperidines the polarization resistance values increase and an additional relaxation time constant appears, which can be related to the formation of intermediate adsorbed species on the electrode surface [32].

Figure 8 shows the Nyquist plots in the absence and presence of various concentrations of piperidine. Two capacitive loops with two time constants, first at high frequency with high polarization resistance (R_1) and the other at low frequency with small polarization resistance (R_2) appear. The total polarization resistance R_p equals ($R_1 + R_2$). Values of inhibition efficiency calculated from R_p are obtained from Eq. 7:

$$IE_I = \left(1 - \frac{R^{o}_{p}}{R_p}\right) \times 100 \quad (7)$$

where R^{o}_{p} and R_p is the polarization resistance in the absence and presence of piperidines, respectively.

These impedance plots can be interpreted by using two time constants. The first one at high frequency is related to an external porous layer, whereas the second, at lower frequencies, is attributed to a more resistive internal layer. In this case, the transfer function is the sum of the corresponding layer impedance [33].

$$\bar{Z}(S)^{-1} = \bar{Y}(S) = \theta\, \bar{Y}_L(S) + (1 - \theta)\, \bar{Y}_{corr}(S) \quad (8)$$

where $\bar{Y}_L(S)$ is the layer admittance and $\bar{Y}_{corr}(S)$ denotes the admittance of the corrosion process which occurs at the substrate/electrolyte interface at the bottom of the "virtual pores" within the film [33].

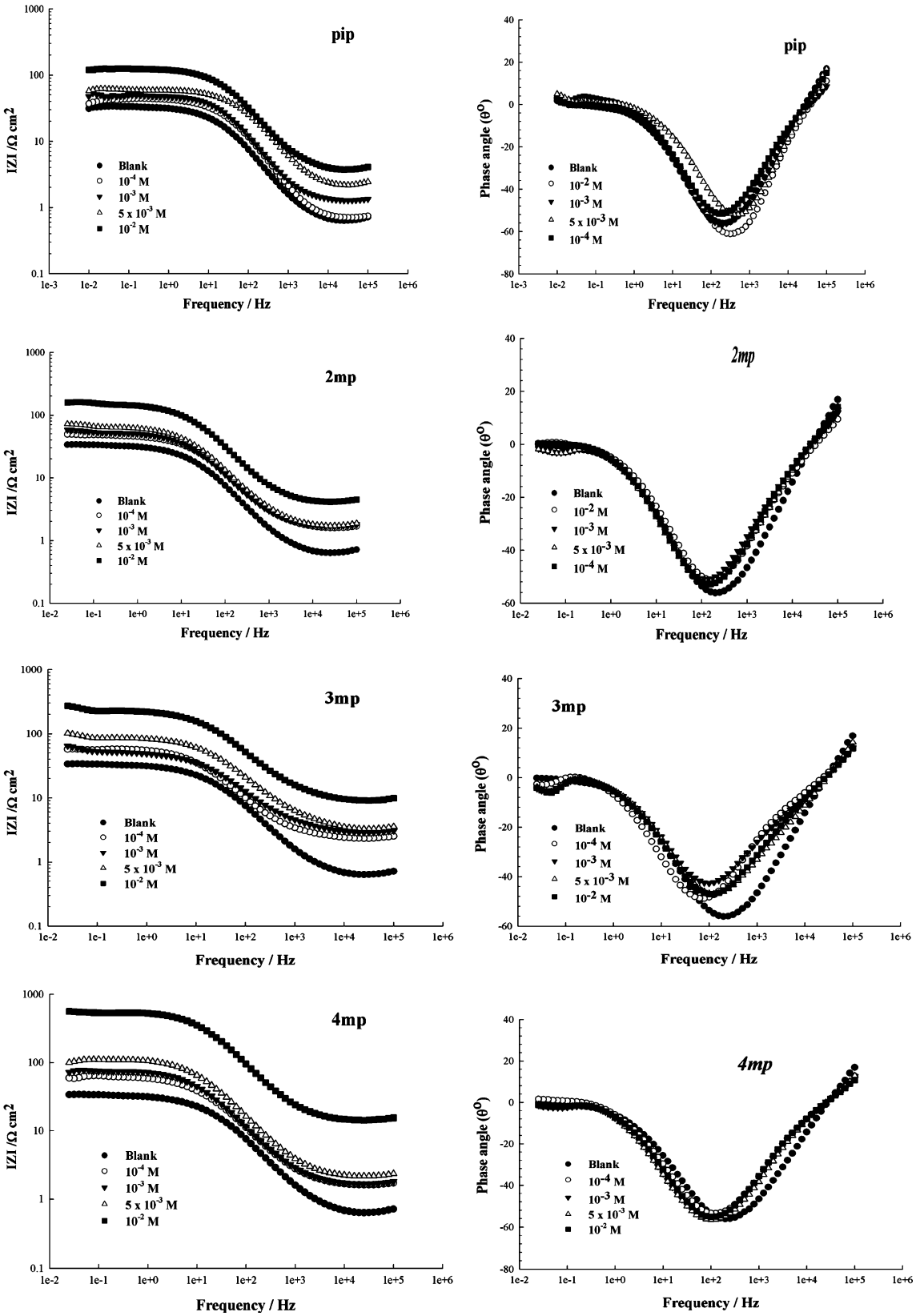

Fig. 7 Bode and Bode phase plots recorded for nickel electrode in 1.0 M HNO_3 solution without and with various concentrations of the four tested inhibitors at the respective corrosion potentials and at 25 °C

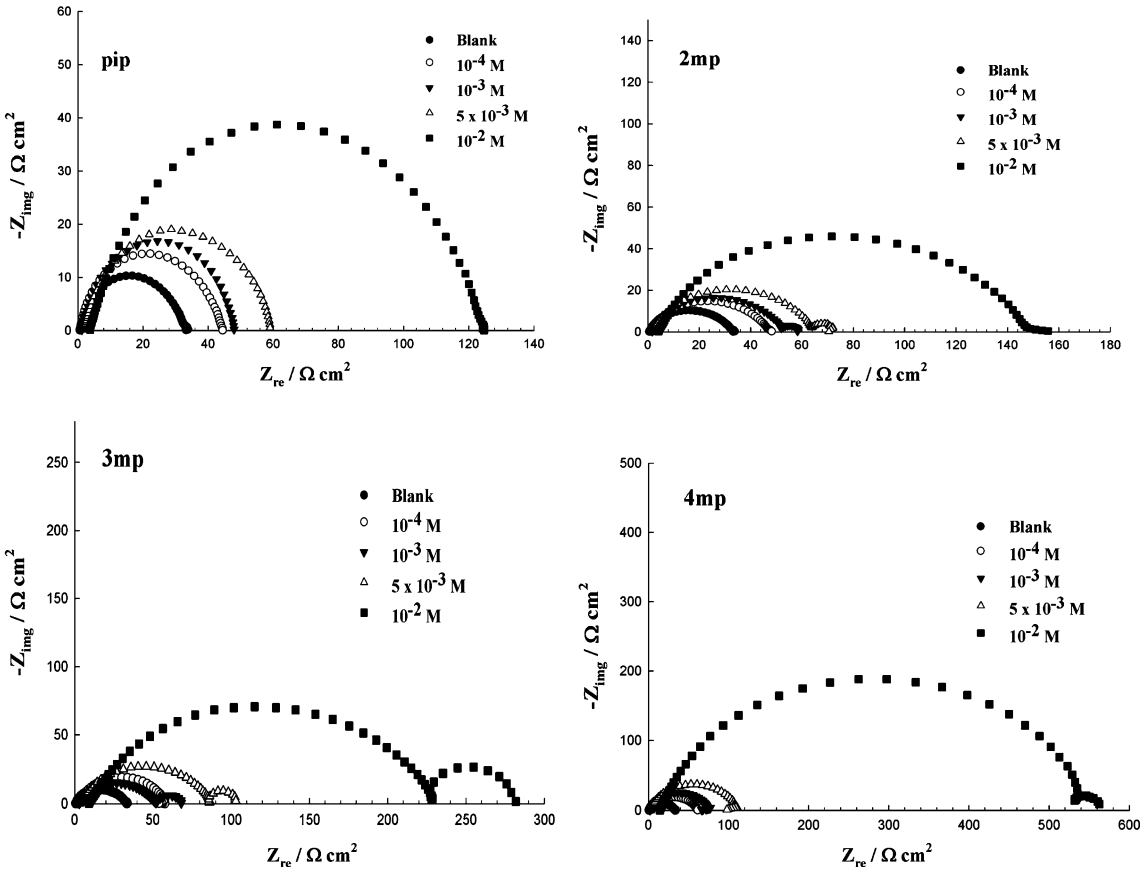

Fig. 8 Complex plane impedance plots recorded for nickel electrode in 1.0 M HNO_3 solution without and with various concentrations of the four tested inhibitors at the respective corrosion potentials and at 25 °C

An equivalent circuit presented in Fig. 9f was used for modelling impedance data obtained in the presence of piperidines. In this circuit R_s is the solution resistance, R_1 and R_2 correspond, respectively; to external and internal layer resistances, and CPE_1 and CPE_2 are constant phase elements. The experimental and fitted data in the presence of 10^{-2} M piperidines after an immersion time of 60 min are depicted in Fig. 9. The CPE is generalised frequency dependant element [34] with impedance given by:

$$Z_{\mathrm{CPE}} = \frac{1}{A(i\omega)^{\alpha}} \tag{9}$$

where A is a frequency independent term, ω the angular velocity and the exponent α value describes circuits elements, so $\alpha = 0$ corresponds to a pure resistor, $\alpha = 1$ to a pure capacitor and $\alpha = 0$ to a Warburg type impedance. Changes in α values have been related to diffusion process, roughness and porosity [33]. The α value in Eq. 9 is less than 1. It is described as *m* and *n* parameters in Fig. 9f and related to CPE_1 and CPE_2, respectively. Values for equivalent circuit parameters are presented in Table 3. In all cases the inhibition efficiency increases with increase in inhibitor concentration. The impedance data listed in Table 3 indicate that the values of both R_1 and $IE_I\%$ increase with increasing inhibitor concentration, while the values of CPEs are found to decrease. This behaviour can be attributed to a decrease in dielectric constant and/or an increase in the thickness of the electrical double layer, suggesting that the inhibitor molecules act by adsorption at the nickel/acid interface [35].

3.4 Mechanism of adsorption

3.4.1 At E_{corr} (Chemical and physical adsorption)

The adsorption of organic compounds can be described by two main types of interactions: physical adsorption and chemisorption. In general, physical adsorption requires the presence of both the electrically charged surface of the metal and charged species in solution. The surface charge of the metal is due to the electric field existing at the metal/solution interface. The surface charge can be defined by the position of the corrosion potential (E_{corr}) with respect to the respective potential of zero charge (PZC) $E_{q=0}$ [36–38]. When the difference $\varphi = [(E_{\mathrm{corr}} - E_{q=0})$ is negative, the

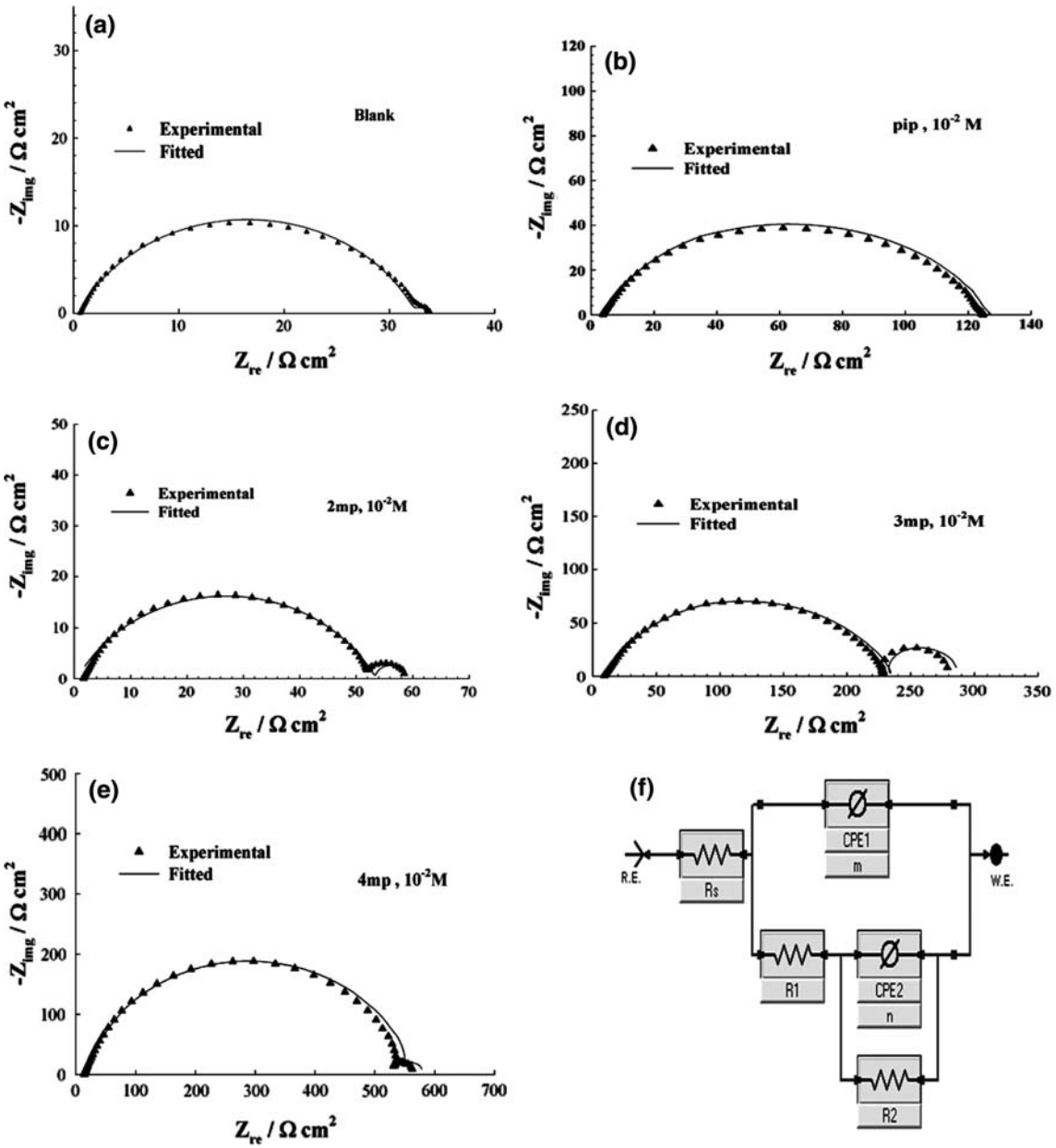

Fig. 9 Fitted and measured impedance spectra obtained from nickel electrode in 1 M HNO_3 solutions without (**a**) and with 10^{-2} M of the four tested inhibitors (**b**, **c**, **d**, **e**) and equivalent circuit (**f**)

electrode surface acquires a negative net charge and the adsorption of cations is favoured. On the contrary, the adsorption of anions is favoured when φ becomes positive. A chemisorption process, on the other hand, involves charge sharing or charge-transfer from the inhibitor molecules to the metal surface to form a coordinate type of a bond. This is possible in the case of a positive as well as a negative charge of the surface. The presence of a transition metal, having vacant, low-energy electron orbitals and of an inhibitor with molecules having relatively loosely bound electrons or heteroatoms with a lone pair of electrons is necessary [39, 40].

It has been shown in the literature that ac impedance studies can be used to evaluate the potential of zero charge (PZC) from the capacitance (C_{dl}) versus voltage (E) plot [36–38, 41]. Figure 10 represents the variation of C_{dl} with E recorded for nickel in 1.0 M HNO_3 solution in the absence (curve 1) and presence of 10^{-2} M 2mp, (curve 2). The minima on the C_{dl} versus E curves are considered as the value of PZC of the electrode. In the region around the PZC the inhibitor molecules in the solution replace the water molecules and the capacitance decreases. When the potential exceeds that of the passivation region, metal dissolution occurs, so that the capacitance increases

Table 3 Circuit elements R_s, R_1, R_2, CPE_1 and CPE_2 values for the equivalent circuit presented in Fig. 9f for nickel electrode in 1.0 M HNO_3 solution without and with different concentrations of the four tested inhibitors

Inhibitor type	Conc./M	R_s Ω cm^2	R_1 Ω cm^2	CPE_1 μF cm^{-2}	*m*	R_2 Ω cm^2	CPE_2 F cm^{-2}	*n*	IE_I%
	Blank	0.6	32	15.72	0.89	1.7	5.90	0.75	
pip	10^{-4}	0.7	43.3	11.67	0.87	0.8	5.25	0.89	23.58
	10^{-3}	1.3	48.25	10.47	0.75	2.5	4.01	0.75	33.59
	5×10^{-3}	2.25	59	8.54	0.85	3.0	3.34	0.91	45.64
	10^{-2}	3.8	124.8	4.037	0.78	1.3	7.72	0.79	73.0
2mp	10^{-4}	1.58	46.61	10.82	0.78	2.1	4.78	0.85	30.81
	10^{-3}	1.7	52.04	9.68	0.91	6.5	1.54	0.86	42.43
	5×10^{-3}	1.7	63.93	7.88	0.87	8.1	1.24	0.84	53.21
	10^{-2}	4.15	148.8	3.38	0.86	13.1	0.76	0.86	79.18
3mp	10^{-4}	2.348	57.15	8.81	0.87	0.5	20.1	0.87	41.54
	10^{-3}	2.7	51.83	9.72	0.79	17.1	0.58	0.78	51.10
	5×10^{-3}	3.4	86.0	5.85	0.75	15.1	0.66	0.79	66.66
	10^{-2}	9.17	227.7	2.21	0.79	54.1	0.18	0.76	88.04
4mp	10^{-4}	1.7	61.45	8.20	0.74	2.07	4.85	0.77	46.94
	10^{-3}	1.6	73.88	6.82	0.75	2.7	3.72	0.78	55.99
	5×10^{-3}	1.93	109.2	4.61	0.91	1.12	9.13	0.85	69.45
	10^{-2}	1.45	534.1	0.94	0.89	28.3	0.35	0.90	94.00

sharply. It is obvious from Fig. 10 that the surface charge of nickel in nitric acid solution at the free corrosion potential is negative ($\varphi = [-(0.00192) - (0.037) = -0.0562$ V(SCE)]). The inhibitors under investigations are organic bases which protonize in an acid medium, affecting the N atom as follows:

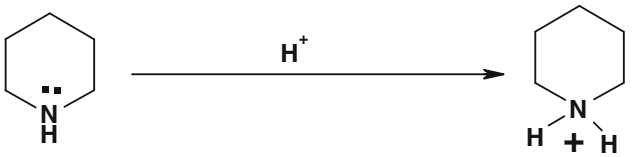

Thus the inhibitor molecule becomes a cation (protonated N-atom), existing in equilibrium with the corresponding molecular form (unprotonated N-atom). Therefore, it can be assumed that protonated piperidine molecules are able to electrostatically adsorb on the negatively charged nickel surface via the positive charge of the N atom (see Fig. 11a).

Due to this electrostatic adsorption, part of the negative charges on the metal surface are shielded, which causes the PZC to shift positively (see curve 2 in Fig. 10). In addition to the physical adsorption, there should be chemical adsorption owing to the coordinate bonds formed between the lone electron pairs of the N-atom and the empty orbitals of nickel atoms which enhance the attraction between the piperidine molecules and electrode surface (Fig. 11b). The adsorption monolayer of piperidines become more ordered and denser with increasing concentration, so the cathodic reduction and anodic dissolution reactions are inhibited significantly.

3.4.2 *In the passive region (adsorption via hydrogen bonding)*

Most previous research has concentrated on relationships between the chemical structure of the inhibitor and inhibition performance. Few investigations have additionally emphasized the importance of the nature of the metal surface [42–44]. Other studies have considered the adsorption of inhibitors to be primarily physical adsorption and/or chemisorption [46, 47]. Few investigations have shown that adsorption could also occur through hydrogen bonding [42–44]. Adsorption via hydrogen bonding predicted by theoretical studies (Table 1) encouraged us to confirm it practically. For this purpose we studied the adsorption behaviour of *2mp*, as an example, on nickel covered with a passivated oxide film, where a hydrogen bond may be formed between the H-atom of the N–H linkage and the oxygen atoms of the passive film [42–44]. Three impedance runs (Fig. 12) were recorded for a nickel electrode in 1.0 M HNO_3 solution containing 10^{-2} M *2mp* at the E_{corr} and at $E_{corr} + 0.20$ V(SCE), i.e., within the potential range of the passive region.

It is obvious from Fig. 12 that in the passive region (curve c) the impedance is higher than that recorded in the active region (curve b). The presence of *2mp* increases the impedance but does not change other aspects of the behaviour. It inhibits corrosion primarily through adsorption on the metal surface. Adsorption of the *2mp* molecules in the active region may occur on reaction intermediates (may be $Ni(OH)_{ads}$) that are only loosely held by the

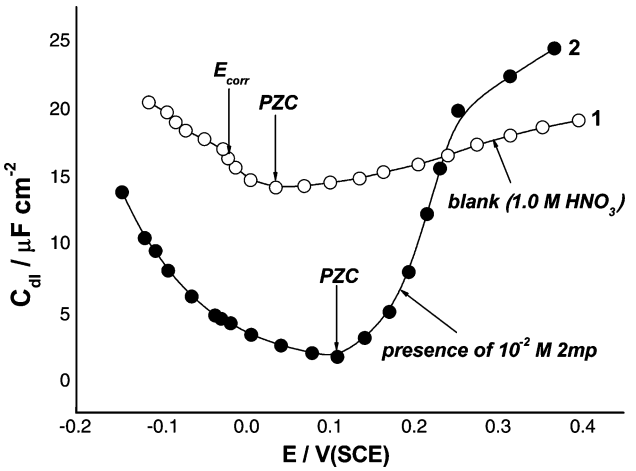

Fig. 10 Capacitance vs voltage plots recorded for a nickel electrode in 1.0 M HNO_3 solution in the absence (curve 1) and presence of 10^{-2} M 2mp at 25 °C

substrate. The adsorbed layer lacks the mechanical stability for good inhibition. In contrast, the metal surface in the passive region is marked by the coverage of oxide films of outstanding mechanical properties [13]. Compact and coherent *2mp* overlayers may therefore be formed which reinforce the capability of the underlying oxide layer to resist chemical attack from aggressive agents, corresponding to increased impedance.

Adsorption in this case is assisted by hydrogen bond formation between *2mp* and oxidized surface species (Fig. 11c). This type of adsorption should be more prevalent for protonated N-atoms, because the positive charge on the N-atom is conductive to the formation of hydrogen bonds. Unprotonated N-atoms may adsorb by direct chemisorption (Fig. 11b) or by hydrogen bonding (Fig. 11c) to a surface oxidized species. The extent of adsorption by the respective modes depends on the nature of the metal surface. Adsorption by direct chemisorption, for unprotonated N-atom, on an exposed metal atom is more probable in the active region. In this region, although the unprotonated N-atom can interact with oxidized metal and the corrosion intermediates by hydrogen bonding, little is contributed to corrosion inhibition because corrosion intermediates and surface oxides cannot form a stable compact layer on the metal surface. Effectual inhibition is predominantly provided by the direct coordination of unprotonated N-atom to metal atoms. In the passive region, where the metal surface is covered by an adherent oxide protective layer, the direct coordination of nitrogen to an exposed metal atom is a remote event. Protonated and unprotonated N-atoms are adsorbed onto the metal through hydrogen bond formation. These results confirm the importance of hydrogen bonding in effective corrosion inhibition in the passive region.

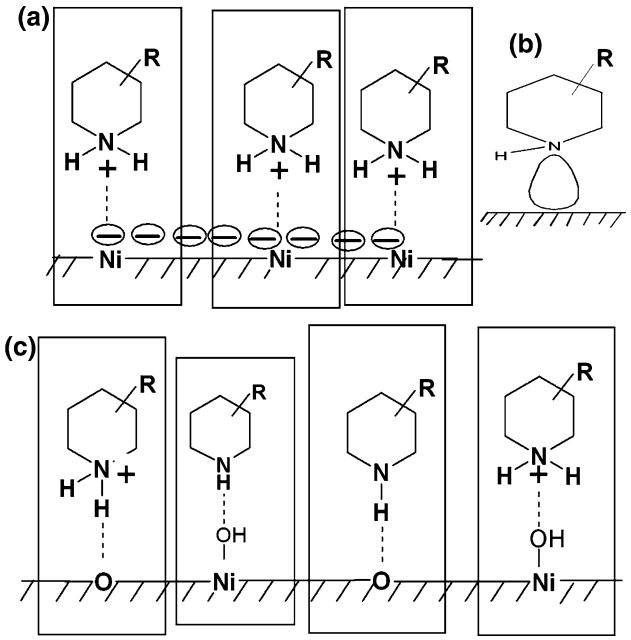

Fig. 11 Mode of adsorption of inhibitors on nickel surface at E_{corr} (the active region), represented by physical adsorption (**a**) and chemical adsorption (**b**), and at E_{corr} + 0.20 V (SCE) (the passive region) (**c**)

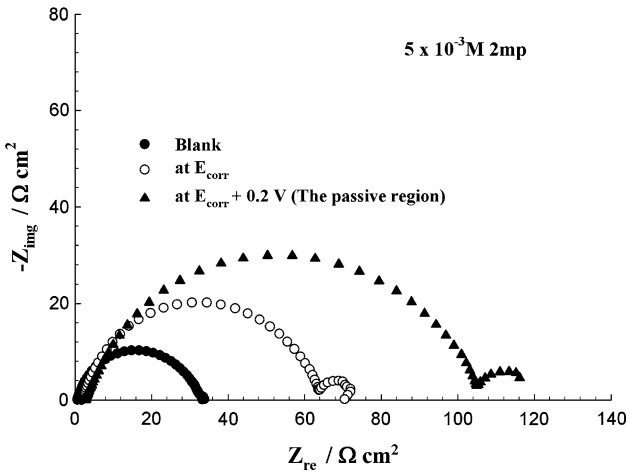

Fig. 12 Complex plane impedance plots recorded for nickel electrode in 1.0 M HNO_3 solution without with 5×10^{-3} M 2mp at 25 °C

4 Conclusions

1. The relationship between inhibition efficiency for nickel in 1 M HNO_3 and the E_{HOMO}, E_{LUMO}–E_{HOMO}, and ΔN of piperidines were calculated by the ab initio method. The inhibition efficiency increased with increase in E_{HOMO} and decrease in E_{LUMO}–E_{HOMO}. 4-methyl piperidine had the highest inhibition efficiency because it had the highest HOMO energy and ΔN values and was the best one capable of offering electrons to the nickel surface.

2. Piperidine derivatives have a very good inhibitive effect for the corrosion of nickel in 1 M HNO_3 solution.
3. Tafel polarization studies have shown that the selected compounds suppresse both anodic and cathodic process and thus acts as mixed-type inhibitors.
4. Impedance results indicate that the value of CPEs tends to decrease and both polarization resistance and $IE_I\%$ tend to increase with increasing inhibitor concentration. This can be attributed to an increase in thickness of the electrical double layer.
5. The effectiveness of piperidines and their derivatives as corrosion inhibitors in 1.0 M HNO_3 solution does not only depend on their molecular structure, but also on the nature of the metal surface. Inhibition is accomplished by adsorption on the metal surface without changing the chemistry of corrosion. The nature of the metal surface can be deterministic of the performance of the inhibitors. Adsorption in the active region of nickel corrosion is based on physisorptive as well as chemisorptive interactions between the inhibitor and exposed metal atoms. As the metal surface is extensively oxidized in the passive region, inhibitor molecules can coordinate with the oxidized surface through hydrogen bond formation.

References

1. Li QK, Zhang Y, Chu WY (2002) Comput Mater Sci 25:510
2. San-Miguel MA, Rodger PM (2000) J Mo Struct (Theochem) 506:263
3. Bartley J, Huynh N, Bottle SE, Flitt H, Notoya T, Schweinsberg DP (2003) Corros Sci 45:81
4. Takahashi M, Qi Y, Nitta H, Nishikawa N, Ohno T (2004) Sci Tech Adv Mater 5:673
5. Khaled KF (2008) Electrochim Acta 53:3484
6. Went W, Feller HG (1970) Z Metallik 61:178
7. Garz I, Glazer B (1974) Corros Sci 14:353
8. Kesten M, Sussek G, Werk U (1976) Korros 77
9. Barkalatsora LA, Pshenicknikov AG (1976) Electrochimiya 12:42
10. Nobe K (1975) MITS Gov. Rep. Announc. Index US. vol 75, p 71
11. Singh MM, Kumar A (1995) Portugaliae Electrochim Acta 3:173
12. Kumar A, Patnaik SK, Singh MM (1998) Mater Chem Phys 56:243
13. Stupniek-Lisac E, Karulin M (1984) Electrochim Acta 29:1339
14. Said F, Souissi N, Es-Salah K, Hajjaji N, Triki E, Srhiri A (2007) J Mater Sci 42:9070
15. Sun H, Ren P, Fried JR (1998) Comput Theor Polym Sci 8:229
16. Roothaan CCJ (1951) Rev Mod Phys 23:69
17. Thiel W (2000) Modern methods and algorithms of quantum chemistry (NIC Series) vol 3, p 261
18. HyperChem, Hypercube, Inc., Gainesville, 2002.
19. Wolinski K, Hinton JF, Pulay P (1990) J Am Chem Soc 112:8251
20. Dewar MJS, Liotard DA (1990) J Mol Struct (Theochem) 206:123
21. Leunberger DG (1973) Introduction to linear and non-linear programming. Addison-Wesley, Don Mills, Ont
22. Rodrigues-Valdez LM, Villamisar W, Casales M, Gonzalez-Rodriguez JG, Martnez-Villafane A, Martinez L, Glossman-Mitnik D (2006) Corros Sci 48:4053
23. Lukovits L, Kalman E, Zucchi F (2001) Corrosion 57:3
24. Sastri VS, Perumareddi JR (1997) Corrosion 53:617
25. Duda Y, Fovea-Rueda R, Galicia M, Beltran HI, Zamudio-Rivera LS (2005) J Phys Chem B 109:22674
26. Fang J, Li J (2002) J Mol Struct (Theochem) 593:179
27. Bereket G, Hür E, Öğretir C (2002) J Mol Struct (Theochem) 578:79
28. Zhao P, Liang Q, Li Y (2005) Appl Surf Sci 252:1596
29. Pearson RG (1986) Proc Nati Acad Sci 83:8440
30. Pearson RG (1988) Inorg Chem 27:734
31. Lukovits I, Kalman E, Zucchi F (2001) Corrosion 57:3
32. Goncalves RS, Azombuja DS, Lucho AMS (2002) Corros Sci 44:467
33. Juttner K (1990) Electrochim Acta 35:1501
34. Stoynov Z (1990) Electrochim Acta 35:1493
35. Khaled KF (2006) Appl Surf Sci 252:4120
36. Amin MA (2006) J Appl Electrochem 36:215
37. Hassan HH, Abdelghani E, Amin MA (2007) Electrochim Acta 52:6359
38. Abd El-Rehim SS, El-Sherbini EEF, Bayoumi RS (2007) Electrochim Acta 52:3588
39. Mehaute AH, Grepy G (1989) Solid State Ionics 910:17
40. Reinhard G, Rammet U (1985) Proceedings of the 6th European Symposium on Corrosion Inhibitors. Ferrara, p 831
41. Lukomska A, Sobkowski J (2004) J Electroanal Chem 567:95
42. Incorvia MJ, Contarini S (1989) J Electrochem Soc 136:2493
43. Karman FH, Felhosi I, Kalman E, Cserny I, Kover L (1998) Electrochim Acta 43:69
44. Braun RD, Lopez EE, Voller DP (1993) Corros Sci 34:1251
45. Banejee G, Malhotra SN (1992) Corrosion 481:10
46. Antropov LI (1962) The 1st International Congress of Metallic Corrosion. Butter worths, London, p 147
47. Aramaki K, Uehre J, Nishihare H (1990) Proceedings of the 11th International Corrosion Congress, vol 3, Florence, Italy p 331